Conf-780813--9

LA-UR -78-1219

MASTER

TITLE: A SHOCK INITIATION STUDY OF PBX-9404

AUTHOR(S): Jerry Wackerle
R. L. Rabie
M. J. Ginsberg
A. B. Anderson

SUBMITTED TO: H. D. P. Symposium
Paris, France

August 28, 1978

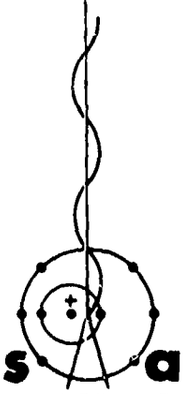

los alamos
scientific laboratory
of the University of California
LOS ALAMOS, NEW MEXICO 87544

Form No. 836
St. No. 2629
1/75

UNITED STATES
ENERGY RESEARCH AND
DEVELOPMENT ADMINISTRATION
CONTRACT W-7405-ENG. 36

A SHOCK INITIATION STUDY OF PBX-9404

Jerry Wackerle, R. L. Rabie, M. J. Ginsberg, and A. B. Anderson
Los Alamos Scientific Laboratory, Los Alamos, New Mexico 87545, USA

Pressure-field histories during the sustained and short-duration shock initiation of PBX-9404 explosive (plastic-bonded HMX) have been determined with embedded Manganin gauges. Numerical integration of the conservation relations and an assumed equation of state are used to obtain the decomposition histories during the initiation process. In both cases, this process is effected by reaction originating near the impact face producing pressure pulses that overtake the shock front and enhance its strength, leading to an abrupt transition to detonation. Correlation of reaction rates to state variables suggest an Arrhenius rate form, modified to include a dependence on shock strength and an induction time. This rate is used in computer simulations of several other initiation experiments on PBX-9404.

I. INTRODUCTION

The planar shock initiation of the plastic-bonded HMX explosive PBX-9404 has been the subject of numerous experimental and theoretical investigations. Experimental studies have established the dependence on input shock strength of the times and distances for buildup to detonation,[1,2] or "Pop-plot" data, and have provided measurements of how these parameters increase with short-duration shock inputs.[3,4] Other previous observations have included determinations of the free surface motion,[5] pressure histories,[6] and particle-velocity histories[7] in inert materials due to waves transmitted from shocked explosive samples of thickness less than the run distance to detonation. Theoretical studies on PBX-9404 have centered mainly on computer simulation of these observations with one-dimensional numerical hydrocodes.[4,8-10] Such computations require a reactant-product equation of state for the explosive and relationships between decomposition rates and the other bulk state variables. Such "rate laws" are developed either by an analysis of shock build-up behavior or, more commonly, are based on theoretically postulated forms, with various constants empirically adjusted to obtain the best simulation of observations.

Recently, more detailed information on the shock-induced decomposition and initiation of PBX-9404 has been provided by measurements with embedded Manganin pressure gauges.[9,11] Such data not only make more stringent demands on the postulated rate laws, but also allow a procedure for deriving them. In this procedure, the gauge data are used to establish a pressure-field history during an initiation experiment, and a direct, or Lagrangian, analysis is used to calculate the density- and energy-field histories.[12] Assumption of a reactant-product equation of state allows calculation of the decomposition and reaction rates over the space-time region covered by the analysis. If a position-independent correlation of the rates to other state variables (and their rates of change) can be found, an empirical rate law can be formulated. Used in a computer simulation (with the same equation of state), such a rate dependency should at least return the observations producing it. If the analyzed experiments include a large enough range of thermodynamic conditions, and if judicious consideration is made of supplemental initiation and detonation information on the explosive, the rate formulation may be effective for the computer simulation of experiments quite different from those used to obtain the rate law.

In this paper we report the use of such a procedure to derive an empirical rate law for the shock-induced decomposition and initiation of PBX-9404. As described in the next Section, the necessary experiments were performed at a single shock strength, using both sustained and short-duration shock conditions to initiate the explosive. In Section III, the direct analysis of these experiments is presented, and the decomposition dynamics of the two cases compared. The correlation of the calculated reaction rates to pressure and temperature is examined and an empirical rate law is formulated in Section IV. The ability of this rate form to yield computer simulations of both our observations and many of those cited earlier is demonstrated in Section V and discussed in Section VI.

II. EXPERIMENTS

Our experimental methods were similar to those reported for our previous study of high-density PETN.[12] The specific arrangement used for embedded-gauge measurements in PBX-9404 is shown in Fig. 1. The copper flyer and a 0.55-mm/μs projectile velocity provided a 2.9-GPa input shock strength in all experiments. A solid aluminum projectile faced with an 8-mm copper plate was used in the sustained shock experiments. The explosive target assembly was changed from the multilayer configuration used previously to allow gauges to be located at four different levels without requiring the reactive shock to transit more than one gauge assembly. Gauges were located at positions between 1 and 8 mm from impact, all less than the ∿10-mm distance to detonation expected with a sustained, 2.9-GPa input.

The same, 50-Ω, Manganin-grid gauges were used as in our previous work, yielding pressure measurements with about 5% accuracy.[13] As discussed in a note added to Ref. 12, such gauges have given records with consistent, but anomalous, premature pressure maxima, apparently due to shunt conductivity in the gauge assembly. This artifact initially led us to believe that decomposition of PETN was interrupted when only partially reacted. We believe we have avoided this error with PBX-9404 by using thicker plastic insulation (0.1 mm instead of 0.05 mm) in most instances, and in not using late stages of the records in the analysis. As seen in the next Section, we find no evidence of "interrupted decomposition" in the present work.

Gauge records for the sustained-shock experiments, shown later in Section IV, display the pressure excursions similar to those for high-density PETN, rising more rapidly and attaining higher values as the depth into the sample increases. Shock-front amplitudes also increase with depth, consistent with previous explosive-wedge[2] and wave-transmission[7] observations.

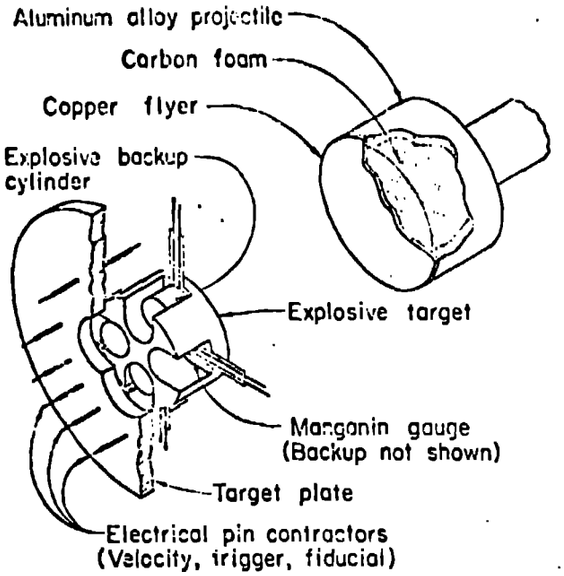

Fig. 1. Arrangement for embedded-gauge experiments.

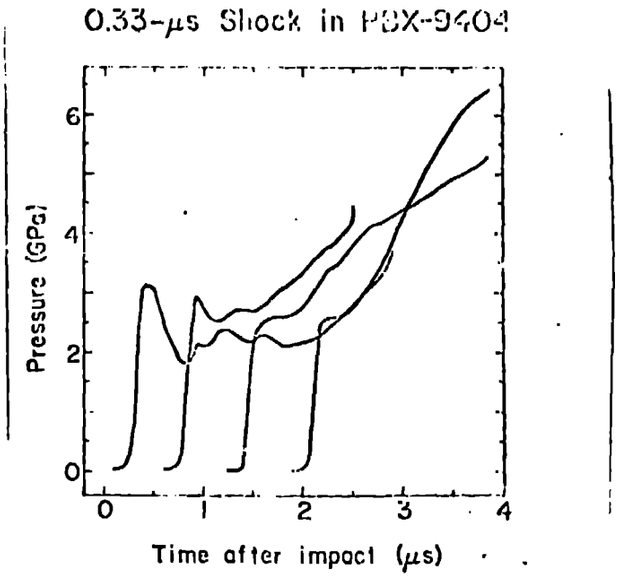

Fig. 2. Typical pressure histories.

Pressure histories for a 0.33-μs pulse (defined as the time for the lead rarefaction to enter the explosive), generated with a 0.76-mm flyer, are shown for nominal 1-, 3-, 5-, and 7-mm depths in Fig. 2. Here the shock strength is seen to decay over the run distance covered, again consistent with earlier observations.[7] However, after an initial decay due to the overtaking rarefaction, the pressure profiles all show an increase, presumably due to decomposition. It was assumed that given enough run distance, this input condition would lead to initiation of the PBX-9404. This was confirmed with an explosive wedge experiment, that showed the 0.33-μs pulse produced a modest decay in the shock front in the first 10 mm of run, followed by a growth and an abrupt transition to detonation at ∿14.5 mm.

To complete the information needed for the direct analysis, impact-face pressure histories were obtained by mounting explosive samples on the gun projectiles and firing them into copper targets faced with Manganin-gauge assemblies. For the sustained-shock case, this pressure record also provided an impact-face particle-velocity history, as this parameter must follow the known compression isentrope for copper. This is not true in the short shock case. Consequently, we measured the free-surface velocity history of a 0.76-mm copper plate struck with a PBX-9404 flyer, using the streak-camera reflection technique.[5] Neglecting the compression of the copper flyer, this determination approximates the impact-face velocity history needed in the direct analysis.

III. DIRECT ANALYSIS AND DECOMPOSITION DYNAMICS

Our direct analysis of the gauge data is an improved version of that described in Ref. 12. The pressure-field histories, $p(h,t)$, are defined in Lagrangian coordinates by interpolation through the pressure-time records afforded by the gauges. Evaluation of pressure gradients and time integration of the momentum conservation relation provide the velocity-field histories, $u(h,t)$. Evaluation of the particle-velocity gradients and integrations of the mass and energy conservation relations provide a complete history of the compression and energy fields [$\xi(h,t)$ and $e(h,t)$, where

$\xi = 1 - \rho_0/\rho$, ρ being the density] over the space-time region covered by data. Our analysis is conducted in a computer program constructed much like a one-dimensional numerical hydrocode, with the space scale of the observations divided into small (typically 0.03-mm) increments or cells, and the conservation relations numerically integrated in small (typically 10-ns) time cycles. The gauge records are idealized as sharp shocks and fitted with smooth functions. State variables at the shock front are constrained to evolve as determined by empirical fitting of gauge and explosive-wedge data and as specified by the Hugoniot relations and the known, unreacted Hugoniot for PBX-9404.

The analysis is quite sensitive to the interpolation of the pressure data between a few gauges. With pressures specified by data, the computation of the decomposition field, $\lambda(h,t)$ (where $\lambda = 0$ for unreacted and $= 1$ for fully reacted), becomes dependent upon the calculated compression histories, which in turn essentially depend on the second derivative, or curvature, of the pressure-distance profiles. In our present analysis, the slopes of the pressure-distance profiles are constrained at the endpoints (using momentum conservation and velocity histories at the impact face and shock-change relations and the assumption of no reaction at the shock front), but are arbitrarily fitted with cubic splines in the interior. Such algorithms minimize the magnitudes of the curvatures, and thus reduce unwanted excursions in the calculated compressions; however, this imposes no physical constraints on the compressions. Along with measurement error, this is responsible for some anomalies in the compression and decomposition profiles and the scatter in the reaction rates shown later.

The principal improvement to our analysis is the addition of various equation-of-state formulations to the computer program, allowing the convenient calculation of the degree of decomposition and reaction rates. In the work reported here, we used Mader's HOM equation of state.[8] In this representation, Mie-Grüneisen forms describe both the unreacted solid and fully reacted products, using, respectively, the shock Hugoniot and a BKW calculated isentrope as reference loci. Constant specific heats are assumed for both components. The reactant-product mixture is determined by the assumptions of ideal mixing of both specific volume and energy and of pressure and temperature* equilibrium between the two phases. The HOM constants used for PBX-9404 are the same as those described in Ref. 8, except that we employ an unreacted, rather than the reactive, Hugoniot for the solid. We use the shock velocity-particle velocity relation

$$U = 2.423 + 1.883\,u \qquad (\text{mm}/\mu\text{s}) \ .$$

Eight pressure histories for the sustained-shock experiments and six gauge records for the short-duration input were used in the direct analysis of experiments described in Section II. The pressures, compressions and decompositions determined are compared in Fig. 3. These variables are displayed in the laboratory (Eulerian) distance frame, in snapshots taken at 0.25-μs intervals, with the last profile at 2.5 μs after impact. The dashed curves indicate the evolution of the shock front.

The sustained-shock initiation behavior displayed should be recognized as that characteristic of heterogeneous explosives. Decomposition occurs first near the impact face, following an induction time after shock passage. A pressure pulse is formed near the impact face, grows and propagates

---

*While this formulation of temperature is sensible in a homogeneous material, for heterogeneous explosives it is, at best, an ill-defined average parameter, and probably much lower than the temperatures of the hotspots dominating the decomposition.

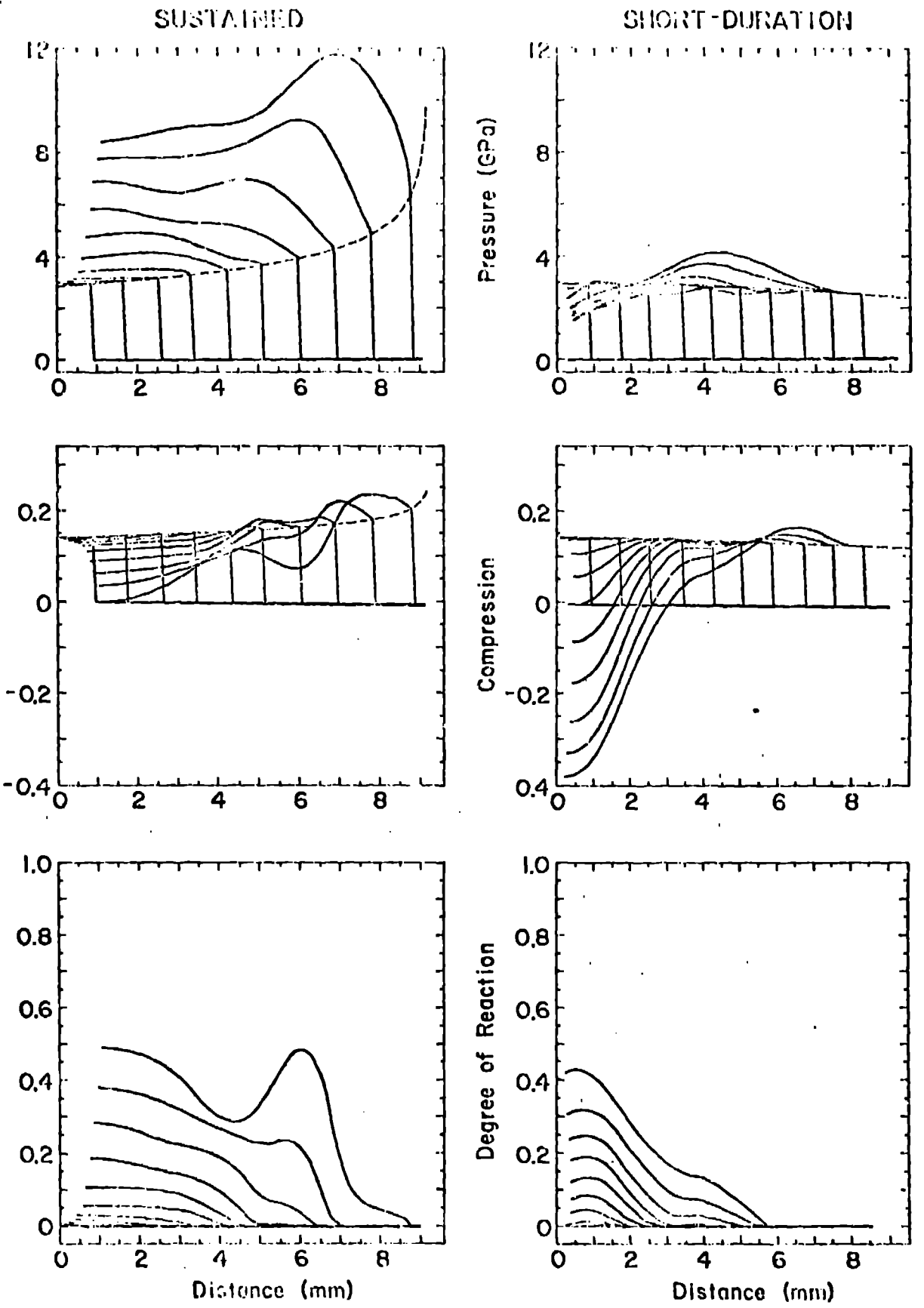

Fig. 3. Comparison of calculated pressure, compression and decomposition profiles for sustained and short-duration shocks in PBX-9404.

forward, overtaking the shock front and increasing its strength. As the shock amplitude grows, the induction time for the onset of decomposition is reduced and the reaction rate (as manifested by the separation in decomposition profiles) is substantially increased. This results in the abrupt transition to detonation at the shock front. With this transition occurring about 1 mm and 0.2 μs beyond the last (2.5-μs) profile, it seems likely that full reaction occurs at the front before being attained near the impact face. While the impact-face decomposition is being slowed somewhat, probably due to the depletion factor, there is no indication it will be interrupted. The compression picture during the sustained-shock initiation process is one of modest expansions near the impact face, due to deceleration of the projectile, and of a compressed region near the shock front due to the pressure pulse advancing into relatively confined material. The late-time dip in the compression profile around 4 mm from impact and the accompanying structure in the reaction profiles may well be anomalies of the direct analysis.

The striking feature of the short-duration shock analysis is that the decomposition produced near the impact face is comparable to that produced by the sustained input. However, with the thin flyer providing little confinement, the effect of the reaction is to expand the explosive, holding the pressures to relatively modest levels, and initially allowing the shock front to decay. Presumably, as reaction occurs deeper within the explosive, self-confinement will allow formation of a more substantial pressure pulse, which--at an added run distance--will overtake and strengthen the shock front and effect the transition to detonation much as with a sustained shock. Unfortunately, our present gauge data do not cover a sufficient spatial range to demonstrate this process.

The comparisons in Fig. 3 alone provide a fairly descriptive view of the shock initiation process in PBX-9404, and emphasize the dominant role of the shock strength, and the relative unimportance of subsequent pressure history, in determining the decomposition behavior. These features will become more evident in the following Section.

IV. DECOMPOSITION RATE CORRELATIONS AND EMPIRICAL RATE LAW

Reaction rates, divided by the depletion factor, $(1-\lambda)$, were derived from the direct analysis of our two cases and are plotted against pressure and temperature in Fig. 4. The strings of symbols are calculated at the indicated distances from impact at 0.1-μs time intervals, with time generally increasing as the rates increase.

Examination of the pressure correlation of the sustained-shock experiment shows that after an induction time, the calculated rates lie in a reasonable band, implying that a simple pressure-dependent rate would treat this case. The curve drawn on the graph is the Forest Fire form that has provided good computer simulations of a variety of strong shock initiation and detonation failure observations.[8] This rate formulation was developed through considerations of single-curve buildup and the effect of decomposition on shock front evolution; it is calibrated to Pop-plot data, and consequently to more compressed, lower temperature conditions that we have in the later stages of our experiments. Forest has used his rate in a computer simulation of our sustained-shock experiment.[14] While the shock front growth was somewhat stronger and the pressure profiles had more of a growing-square-wave character than our observations indicate, the decomposition history was quite similar to that shown in Fig. 3.

With our analysis of substantial reaction at modest--even decreasing--pressures in the short-shock case, it is not surprising that any simple pressure-dependent form fails to correlate to the calculated rates, and particularly not one calibrated to state conditions so remote from those of

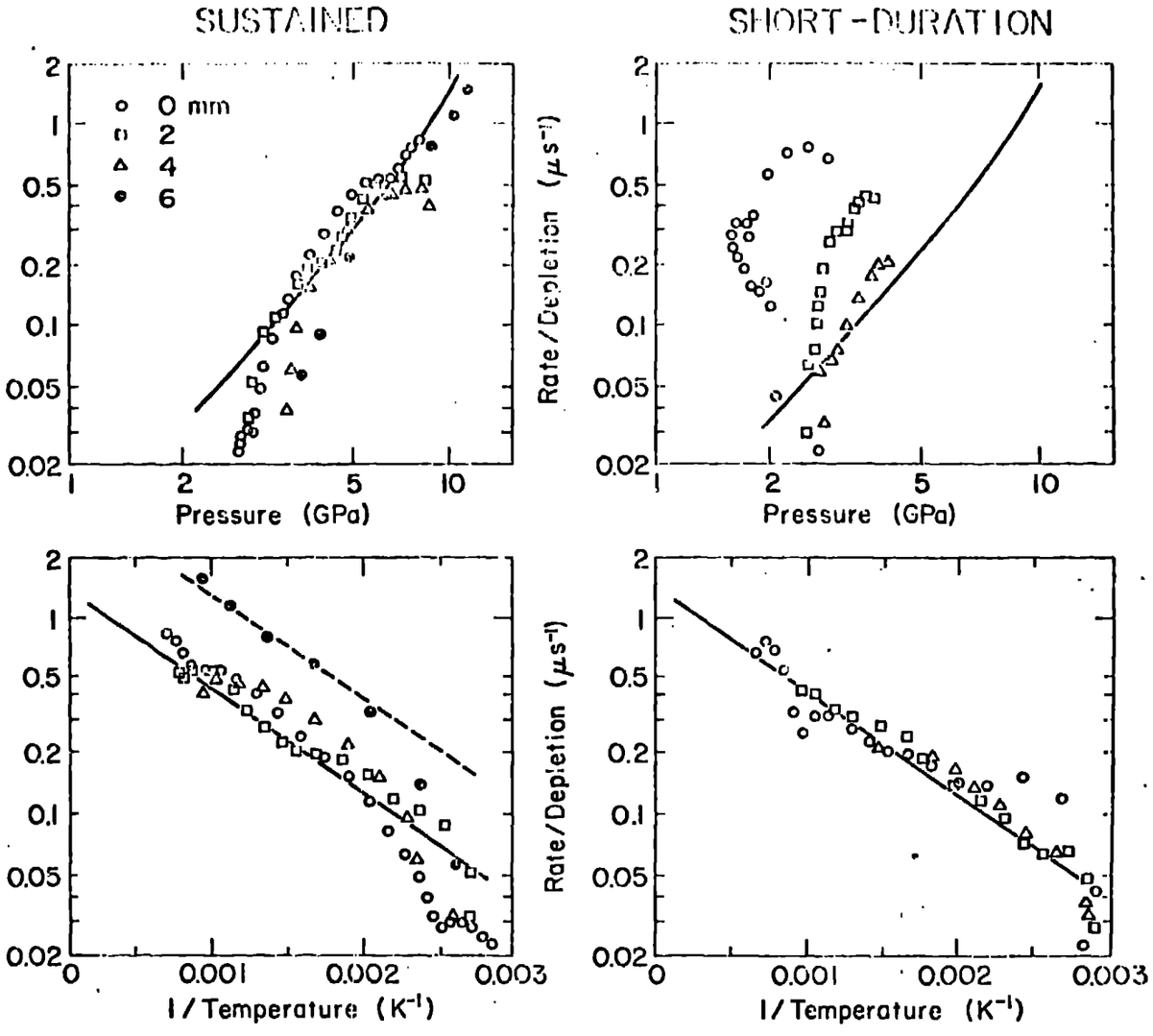

Fig. 4. Correlations of calculated decomposition rates to pressure (above) and temperature.

our experiment as Forest Fire. Computer simulation of our short-shock experiment with this rate gave surprisingly good agreement with our observed 14.5-mm run distance to detonation. However, the pressure and decomposition histories were quite different from those of Fig. 3. The Forest Fire computation gave a relatively modest amount of reaction, triangular-shaped pressure profiles, and a slow, but monotonically-increasing, growth at the shock front.[14]

Correlations of the calculated decomposition rates to temperature are shown in an Arrhenius form. Again allowing for an induction time, most of the decomposition rates for *both* cases lie within a reasonable band, and can be fitted with the same solid line. The expression for this line is

$$\dot{\lambda}/(1-\lambda) = 1.42\ e^{-1200/T} \qquad (\mu s^{-1})$$

where T is the temperature. Two problems with this rate form remain to be corrected. The first is that an induction-time factor needs to be added, and the second is that the rate is much too small for stronger shock problems. For example, a detonation wave in PBX-9404 would have, with the above rate, a ∿1-mm reaction zone thickness, which is known to be an order of magnitude too large. What is needed, of course, is the dependence on shock strength discussed in the previous Section. The form of this dependence is suggested by correlation of rates calculated for the sustained shock 6 mm from impact, indicated by the dashed line in Fig. 4. The fact that this line has the same slope but a larger intercept indicates that we should retain the above activation temperature and increase the pre-exponential with a function of shock strength. Since the shock amplitude after 6 mm run is about 40% higher than at gauges between 0 and 4 mm, and the intercept of the dashed curve is about twice as large as that fitting the other rates, a shock-pressure-squared dependence is suggested.

With these factors considered, our rate form is

$$\dot{\lambda}/(1-\lambda) = Z(p_s)\, G(p,t)\, e^{-1200/T} \quad , \qquad (\mu s^{-1})$$

where

$$Z = 0.17\, p_s^2 \quad , \qquad (\mu s^{-1})$$

and

$$G = e^{-0.5/I} \quad , \quad p > 0.75 \text{ GPa}; \; G = 0, \; p \leq 0.75 \text{ GPa}$$

with

$$I(p,t) = \int_0^t (p-0.75)^2 \, dt' \quad .$$

Here p_s is the shock pressure and the constants are chosen appropriate to time in microseconds and pressures in gigapascals. The factor G was chosen rather arbitrarily to give induction times that are strongly reduced with shock strength, as both our analyses and shock-evolution studies[7] indicate. It provides 90% of the full rate in about 1 μs with a 2.9 GPa pressure and in about 0.05 μs with 10 GPa.

V. COMPUTER SIMULATIONS

Our computer simulations were performed with Fickett's one-dimensional numerical hydrocode, PAD.[15] Particularly valuable features of this program included the automatic adjustment of time cycles to insure stability (especially useful for our projectile-impact problems), an algorithm to locate the shock front (at the cell of maximum artificial viscosity) and determine its strength, and provision for accommodating alternate equations of state. A recently improved version of HOM was used with this last option.[14] We also implemented a few modifications needed for our particular rate law.

Simulations of the two experimental configurations used to calibrate our rate law both gave distances to detonation within 0.5 mm of those observed, and gave the comparisons with selected gauge records shown in Figs. 5 and 6. The agreement is good enough that it is necessary only to indicate the small deficiencies. In the sustained shock case, the calculated shock strength at the 8-mm gauge is slightly lower than that observed, and the calculated pressure excursions--particularly of the deeper gauges--are not as rapid as those measured. Simulations of the short-shock experiments did not give as much reduction in shock strength and in impact-face pressure history as observed.

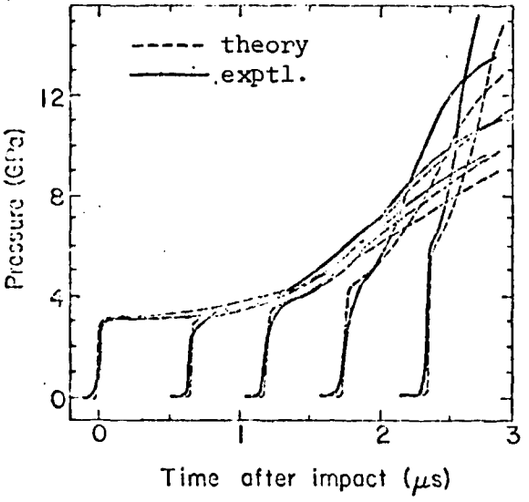

Fig. 5. Comparison of computer simulation (dashed lines) with observation for sustained shock. Gauge sites are nominal 0, 2, 4, 6, and 8 mm from impact.

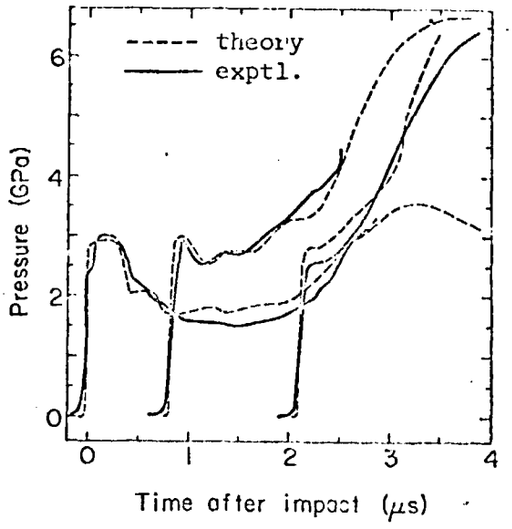

Fig. 6. Comparison of simulation with observation for a 0.33-μs shock input. Gauges are nominally 0, 3, and 7 mm from impact.

In addition to the short-shock configuration used in the analysis, we also performed embedded gauge experiments at 2.9 GPa with 1.02- and 0.51-mm copper flyers. Both of these experiments gave pressure excursions indicative of reaction, and computer simulations of each case gave the same good match to observation, and same slight deficiencies, as obtained with the 0.76-mm flyer.

As noted in the Introduction, if our direct analysis is properly performed and correlations are found, our procedure *should* return computer simulations of the calibrating observations. This is true even if the observations themselves and the assumed state equation are seriously in error! More stringent tests of the rate formulation are afforded by attempts to simulate experiments at shock and state conditions quite different from our own. Our principal such tests were computations of initiation experiments with higher pressure sustained and short-duration shocks, generated with aluminum flyers.

The results of these tests are summarized with reference to Fig. 7. The solid curve is the current best construction of a Pop plot for Los Alamos data on PBX-9404,[2,14] using the unreacted Hugoniot described earlier. Our calculations of sustained-shock distances to detonation, shown without number labels, are in excellent agreement except at 2 GPa, for which we compute a slightly longer run distance. At the right-hand side of Fig. 7 are comparisons with the short-duration shock experiments of Gittings.[3] With a 2.0-mm/μs flyer velocity,* she observed increased excess transit times with

*We have used the reported flyer velocities to determine the shock pressures shown in Fig. 7; pressures given in Refs. 3 and 4 are slightly different due to the use of different Hugoniots.

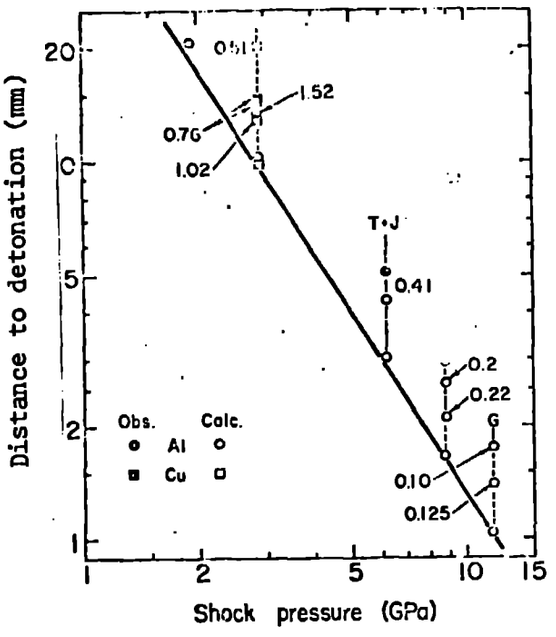

Fig. 7. Pop-plot representation of experiments and simulations for sustained and short-duration shock initiation of PBX-9404.

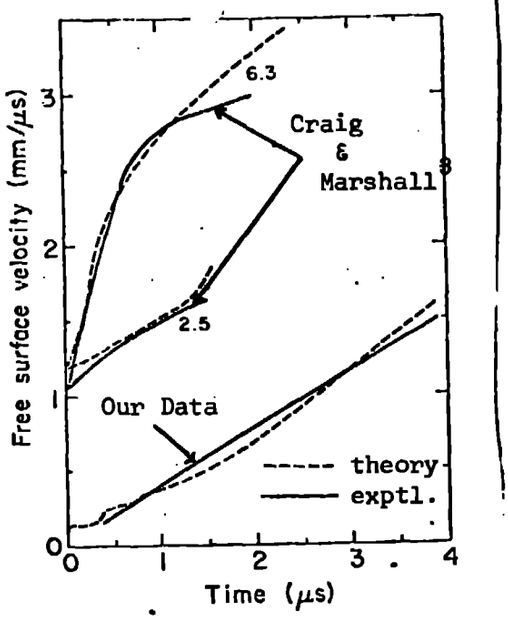

Fig. 8. Simulations (dashed lines) and observations of plate-push experiments with PBX-9404.

0.125-mm flyers and with 0.22-mm flyers with a 1.6-mm/μs velocity. Our computer simulations, labeled with the flyer thickness in millimeters, show increased run distances. However, we do not calculate as large an increase in excess transit time or as sharp a tendency to failure as Gittings' data indicate. Similarly, in our simulation of Trott and Jung's 6.2-GPa experiment,[4] using a 0.41-mm, 1.2-mm/μs aluminum flyer, we calculate a substantially increased run distance, but not as much as observed. Among the points plotted for simulations and the single datum of our 2.9-GPa short-shock experiments is the calculation of a 13-mm run distance for a 1.52-mm aluminum flyer traveling 0.67 mm/μs; this corresponds to an experiment in which buildup to detonation did not occur in a 12.7-mm sample thickness.[4]

Additional tests of our rate formulation were afforded by simulations of two types of "plate-push" experiments, shown in Fig. 8. The first was our observation of a free-surface velocity of a 0.76-mm copper plate struck by PBX-9404, described in Section II. As seen in the lower curves, the simulation is much better than the 5 to 10% error in the experiment. Additionally, the computation showed the impact face velocity history to be nearly identical to that at the free surface, supporting our use of such as assumption in incorporating the measurement in our direct analysis. The upper curves represent our computations of two experiments by Craig and Marshall (see Fig. 4, Ref. 5), in which ∿3-GPa shocks were introduced into 2.5- and 6.3-mm PBX-9404 samples, and the decomposing, but not detonated explosive accelerated 2-mm thick Plexiglas plates. The comparisons are good over most of the observation time; the disparity at late times may be more in our failure to properly simulate their rather complicated high-explosive driving system than in the reaction rate formulation.

Our use of a shock-strength dependence and an induction time in the rate form dictates that the steady detonations calculated in our simulations

are of the Zeldovich-von Neumann-Doering (ZND) form. The HOM equation of state assures computation of a ~54-GPa von Neumann spike pressure and ~36-GPa Chapman Jouget, (CJ) pressure, within the range of accepted values.[16] Calculated ~0.1-mm reaction-zone lengths are also consistent with accepted values. The development of the full ZND configuration typically occurs 0.2 to 0.4 μs after the shock front has reached CJ pressure; attainment of the CJ pressure was used as our criterion for the calculated distances to detonation presented earlier.

VI. DISCUSSION

While our decomposition rate for PBX-9404 is purely empirical, there are strong phenomenological arguments to support some features of the formulation. A principal feature of the rate form is that the decomposition history of the shocked material be predetermined by the strength of the first shock it experiences. Thus, it is conceptually similar to the "nucleation-growth" models favored by other investigators,[9,10,17] and can be justified with the same rationale. The strong evidence given in Section III for such a shock-induced decomposition behavior is supplemented by additional observations on both PBX-9404 and high-density PETN. Quartz-gauge impact-face measurements[12] on thin samples of the latter explosive showed that neither reflected shocks nor returning rarefaction appreciably altered the reaction-induced pressure growth rate,[18] and Kennedy found the same effect in PBX-9404 in the reflected-shock case.[6] In explosive wedge experiments on both compositions, we have found that preshocking with small amplitude precursors increases the run distance to detonation, roughly by the distance required for the second, initiating wave to overtake the precursor.

While use of the second power of the shock pressure in the rate was suggested by our correlations, we were quite prepared to alter this power to get agreement with the Pop plot; this proved unnecessary. The effectiveness of p_s^2 form may in some way be associated with the related correlations of the $p^2\tau$ criterion for short-shock initiation and the approximate p^{-2} dependence of its time to detonation to input shock strength. However, we believe that attaching great physical significance to the power of two is unjustified, particularly in noting that a much larger power is appropriate for the initiation criteria in TATB.[19]

The induction time factor is admittedly the most *ad hoc* aspect of our rate form. Taylor has shown that the induction time for hotspots generated by plastic work at void peripheries is proportional to $\int p^2 dt$.[20] If a finite yield strength is added to his consideration of an ideal viscous fluid, the constant pressure subtracted in our induction time factor can be justified;[21] however, a value as large as 0.75 GPa would require some claims of work hardening. The particular exponential form of our G(p,t) was chosen quite arbitrarily, and the induction time factor of the rate is a major aspect we would hope to better define with improved experiments and analysis.

Several simulations of initiation phenomena in heterogeneous explosives have been done with Arrhenius rate forms, both used arbitrarily[22] and argued on a grain- or hole-burning thesis.[4,17] Since we use a temperature form quite inappropriate for an inhomogeneous material, we find it difficult to believe that this parameter is more than a representation of the average state of the material that fortunately correlates to the decomposition rate. This view was reinforced by our experience in executing the entire analysis/simulation process with the relatively simple BLEND equation of state,[15] as well as a quite different temperature form;[22] the Arrhenius rate correlations and matching of computer simulations were nearly as good as those described above.

While our empirical rate form is not completely satisfying physically, we believe the procedure by which it was derived has been shown to be powerful and effective. As more physical forms are proposed, they can be readily tested and their adjustable constants determined by the same method. This promise provides the impetus for our continuing efforts to improve the range and accuracy of our embedded-gauge measurements and to develop a direct analysis more constrained to the allowed state history in the explosive.

Acknowledgments

We greatly appreciate the discussions and aid of Wildon Fickett, Charles Forest, Jack Jacobson, and James O. Johnson and the support efforts of Beverly Clifford, Tom Elder, Henry Olivas, and Larry Salazar.

References

1. J. B. Ramay and A. Popolato in *Fourth Symposium (International) on Detonation*, Office of Naval Research report ACR-126 (1965), p. 233.
2. B. G. Craig, private communication of Los Alamos Scientific Laboratory internal reports (1970).
3. Elisabeth F. Gittings in Ref. 1, p. 373.
4. B. D. Trott and R. G. Jung in *Fifth Symposium (International) on Detonation*, Office of Naval Research report ACR-184, p. 191.
5. B. G. Craig and E. F. Marshall in Ref. 4, p. 321.
6. J. E. Kennedy in Ref. 4, p. 435 and private communication (1978).
7. J. E. Kennedy and J. W. Nunziato, J. Mech. Phys. Solids 24, 107 (1976). See also J. W. Nunziato, J. E. Kennedy and D. R. Hardesty in Ref. 12, p.47.
8. C. L. Mader, Los Alamos Scientific Laboratory report LA-6259 (1976)*
9. E. L. Lee, H. Cheung and C. M. Tarver, Bull. APS Series II, 23, 36 (1978) and L. Green, E. Nidick, E. Lee and C. Tarver, this Symposium.
10. R. Barlett, et al., Bull. APS Series II, 23, 36 (1978).
11. Jerry Wackerle, J. O. Johnson, and M. J. Ginsberg, Bull. APS Series II, 21, 1286 (1976).
12. Jerry Wackerle, J. O. Johnson, and P. M. Halleck in *Sixth Symposium (International) on Detonation*, Office of Naval Research report ACR-221, p. 20.
13. Jerry Wackerle, J. O. Johnson, and P. M. Halleck, Los Alamos Scientific Laboratory report LA-58 (1975).*
14. Charles Forest, Los Alamos Scientific Laboratory internal reports and private communications (1976-1977).
15. W. Fickett, Los Alamos Scientific Laboratory report LA-5910-MS (1975).*
16. [illegible] in Ref. 12, p. 637.
17. A. [illegible] ord, Ref. 12, p. 371.
18. Jerry [illegible] Johnson, Los Alamos Scientific Laboratory report LA-5111 (1973).*
19. R. K. Jackson, et al., in [illegible].
20. J. W. Taylor, Los Alamos Scientific [illegible] internal reports and private communication (1971-1973).
21. Jerry Wackerle, J. O. Johnson, and P. M. [illegible]ries II, 20, 20 (1976).
22. Jack Jacobson and Wildon Fickett, Los Alamos Scientific Laboratory report LA-5915-MS (1975).*

* This report is available from National Technical Information Service
U. S. Department of Commerce
5285 Port Royal Road
Springfield VA, USA, 22161